

Modulation of synchronization dynamics in a network of self-sustained systems



H.G. Enjieu Kadji ^{a,*}, J.B. Chabi Orou ^b, M.A.F. Sanjuán ^c

^a Monell Chemical Senses Center, 3500 Market Street, Philadelphia, PA 19104, USA

^b Institut de Mathématiques et de Sciences Physiques, B.P. 613, Porto-Novo, Benin

^c Nonlinear Dynamics, Chaos and Complex Systems Group, Departamento de Física, Universidad Rey Juan Carlos, Tulipán s/n, 28933 Móstoles, Madrid, Spain

ARTICLE INFO

Article history:

Received 6 February 2013

Received in revised form 5 July 2013

Accepted 8 July 2013

Available online 25 July 2013

Keywords:

Phase synchronization

Self-sustained systems

Local injection

Noise

ABSTRACT

This paper addresses the combined modulatory effects of non-nearest neighbor oscillators and local injection on synchronized states dynamics with their corresponding stability boundaries in a network of self-sustained systems. The Whittaker method and Floquet theory are used to predict analytically the stability of these states for identical and non-identical coupling parameters. Charts revealing the modulation of synchronized states and their stability boundaries at the second order of interaction in the cases of identical and non-identical coupling parameters are constructed with and without an external signal locally injected in the network. Numerical simulations validate and complement the results of analytical surveys. The limits of the stability regions are numerically explored when a small amount of Gaussian white noise is also injected in the network.

© 2013 Elsevier B.V. All rights reserved.

1. Introduction

Coupled nonlinear dynamical systems have become a topic of growing interest since they show very rich phenomena such as synchronization. The synchronization of nonlinear oscillations occurring in networks, such as arrays or rings, is a rather attractive topic due to the enormous variety of potential applications. For instance, arrays of coupled nonlinear oscillators have been used for the description of Josephson-junctions [1], multimodes lasers [2,3], relativistic magnetrons [4]. Furthermore, arrays of oscillators also arise in studies of biological rhythms of the heart [5], nervous system [5,6], intestines [7], pancreas [8] and other biological systems [9–12]. The case of ring coupling topology is also of interest. For example, rings of two neuronal systems have been used to study the mixed inhibitory and excitatory circuit coordinating the motion of lo-cust wings during flight [13]. It has also been demonstrated that in quadrupedal mammals, the four oscillators controlling the limb may be coupled in some form of ring [14,15]. A previous study has investigated different states of synchronization in a ring of mutually coupled self-sustained electrical oscillators [16]. Properties of the variational equations of stability have been utilized to investigate the dynamics of the ring and a stability map displaying domains of synchronization to a locally injected external excitation has been reported. Recently, these results have been validated experimentally and the consequences of parameter mismatch have been also emphasized [17]. But, these studies [16,17] and others [18–20] have considered only the influence of nearest neighbors coupling on stability boundaries using both analytical and numerical investigations. Thus, we want to investigate in this paper the modulatory effect of non-nearest neighbors and the local injection on synchronized states and their corresponding stability boundaries. We analyze first the stability of the synchronization process when both first and second order couplings are considered. Later, we address the question of the

* Corresponding author.

E-mail addresses: hkadji@monell.org, henjieu@gmail.com (H.G. Enjieu Kadji), jchabi@yahoo.fr (J.B. Chabi Orou), miguel.sanjuan@urjc.es (M.A.F. Sanjuán).

synchronization conditions when an external signal is locally injected in the network. The paper is organized as follows. In Section 2, we introduce the system configuration and problem statement. In Section 3, we investigate the impact of the range of interaction on the stability boundaries for identical and nonidentical coupling parameters. Section 4 deals with the influence of a local injection for identical and nonidentical coupling parameters. Conclusions are given in Section 5.

2. System configuration and problem statement

The model shown in Fig. 1 is a ring of N identical mutually coupled self-sustained electrical systems where each unit is modeled as van der Pol oscillator (see Fig. 2). Each van der Pol oscillator consists of a nonlinear resistor NLR , an inductor L and a condenser C , all connected in parallel. The coupling between the units is realized through an inductor L_c . Experimentally, the network can be built using $TL - 082$ operational amplifiers and $AD - 633$ multipliers as reported previously [17].

The volt-ampere characteristic of the nonlinear resistor for the k th unit is expressed by a symmetric cubic nonlinearity, which is illustrated by

$$i_k = -e_1 V_k + e_3 V_k^3, \quad e_1, e_3 > 0; \quad 1 \leq k \leq N. \tag{1}$$

This form of nonlinearity was introduced by van der Pol who had considered a lumped oscillator with two degrees of freedom to discuss simultaneous multi-mode oscillations [21,22]. In such situation, the oscillator traces a particular path through phase space, and if some perturbation excites it out of its accustomed rhythm, it soon returns to its former path. Oscillators that have a standard waveform and amplitude to which they return after small perturbations are known as limit-cycle oscillators (e.g. van der Pol oscillators). As shown in the appendix, the network is described by the following set of second order non-dimensional nonlinear differential equations:

$$\ddot{x}_k - \mu(1 - x_k^2)\dot{x}_k + x_k = K_1(x_{k+1} - 2x_k + x_{k-1}) + K_2(x_{k+2} - 2x_k + x_{k-2}), \tag{2}$$

where x_k stands as the voltage amplitude of the k th oscillator and μ is a positive coefficient of nonlinearity. K_1 and K_2 are the coupling strengths of the first and second nearest neighbors respectively. The model assumes the boundary conditions cyclic

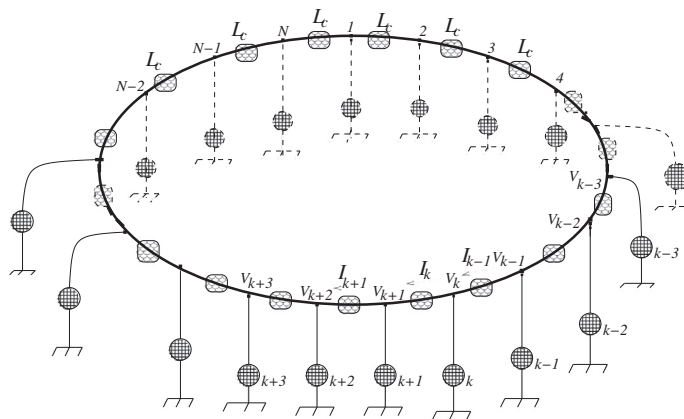


Fig. 1. Network of N mutually coupled self-sustained electrical oscillators.

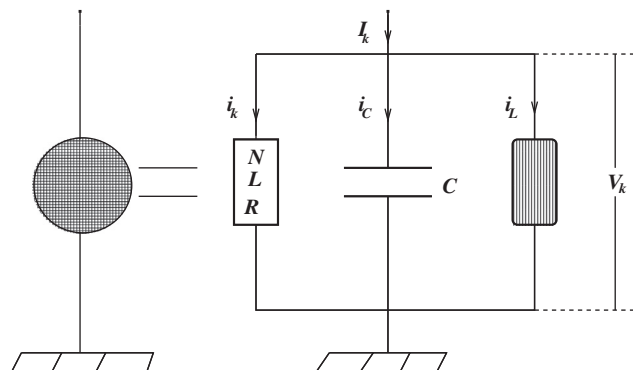


Fig. 2. Model of a self-sustained electrical oscillator.

and defined as $x_{k+N} = x_k$. When $K_2 = 0$ and $K_1 \neq 0$, Eqs. 2 lead to a system of mutually coupled van der Pol oscillators for which only the first nearest neighbors coupling are considered [16,18]. When $K_1 = K_2 = 0$, each unit is uncoupled and can display a variety of phenomena for different values of μ . Such a network possesses several potential applications since van der Pol oscillators are widely used to model different type of biological phenomena [5,23]. Nevertheless, the most common use of these type of oscillators is in engineering, where they are extensively used for example in the study of vibration [24].

Such a network is not merely of theoretical interest, but it has also many different applications. For instance, in electronic engineering, they are useful in determining the dynamical states of microwave oscillators for which the state of each oscillator is influenced not only by first nearest neighbors. Moreover, the model investigated here can be of interest for addressing some biochemical processes. Indeed, limit cycle oscillations have been observed in a Goldbeter's 5-variable model of the biological circadian (approximately 24-h period) clock in the fruit fly *Drosophila* [25]. The fact that the Goldbeter's 5-variable model has been demonstrated to be a biochemical analogue of a van der Pol equation [26] opens other windows of potential applications for the network under consideration. As a first approach in determining the contributions of second order coupling on synchronized states and stability boundaries, and also for convenience, we set $N = 4$.

3. Stability analysis in the network

The phase of a van der Pol oscillator depends on initial conditions. Then, if four identical van der Pol oscillators are initiated with different initial conditions, they will finally circulate on the same limit cycle but with four different phases. Thus, the purpose of the synchronization is to phase-locked those oscillators. Additionally, the model is physically interesting only if its resulting dynamical state is stable, i.e., all the perturbed trajectories return to the original limit cycle. It is therefore particularly important to develop criteria that guarantee the asymptotic stability of synchronization if applications are to be constructed because one can tolerate synchronization to fail but not to be unstable since instability could damage the system. Consequently the stability of synchronization, which means that the process of synchronization is really taking place, would be the most desirable outcome from a technological point of view.

3.1. Analytical survey

We assume the two coupling parameters to be proportional and set $K_2 = \alpha K_1$ where α is a positive parameter quantifying the rate of proportionality. For simplicity, we have chosen $K_1 = K$. Thus, the stability of the resulting dynamical state can be studied by linearizing Eqs. (2) around the unperturbed limit cycle x_0 as follows:

$$\ddot{\xi}_k - \mu(1 - x_0^2)\dot{\xi}_k + [1 + 2K(1 + \alpha) + 2\mu x_0 \dot{x}_0]\xi_k = K(\xi_{k+1} + 2\alpha\xi_{k+1} + \xi_{k+3}), \quad 1 \leq k \leq 4, \quad (3)$$

where $\xi_k = x_k - x_0$ stands for the first order perturbation of x_k . For small values of μ , the behavior of one oscillator can be described by a pure sinusoidal trajectory of the form

$$x_0 = A \cos(\omega t - \phi), \quad (4)$$

where A and ω are respectively the amplitude and the frequency of the unperturbed limit cycle in first approximation. The values of A and ω are obtained for instance by the averaging method ($A = 2.00$, $\omega = 0.999$ for $\mu = 0.100$). This first order approximation gives a fairly good agreement between the analytical and numerical results as reported in Ref. [16]. By introducing in Eqs. (3) the rescaling $\tau = \omega t - \phi$ and the diagonal variables (*Fourier modes*) Θ_k defined as follows:

$$\begin{aligned} \Theta_1 &= \xi_1 + \xi_2 + \xi_3 + \xi_4, \\ \Theta_2 &= \xi_4 - \xi_2 = x_4 - x_2, \\ \Theta_3 &= \xi_3 - \xi_1 = x_3 - x_1, \\ \Theta_4 &= \xi_4 - \xi_3 + \xi_2 - \xi_1 = x_4 - x_3 + x_2 - x_1, \end{aligned} \quad (5)$$

we obtain after some algebraic calculations to the following variational equations:

$$\ddot{\Theta}_k + [2\lambda + F(\tau)]\dot{\Theta}_k + G_k(\tau)\Theta_k = 0, \quad 1 \leq k \leq 4, \quad (6)$$

with

$$\begin{aligned} \lambda &= \frac{\mu}{4\omega} (A^2 - 2), \quad F(\tau) = \frac{\mu A^2}{2\omega} \cos 2\tau, \\ G_1(\tau) &= \frac{1}{\omega^2} (1 - \mu A^2 \omega \sin 2\tau), \\ G_2(\tau) = G_3(\tau) &= \frac{1}{\omega^2} [1 + (2 + 4\alpha)K - \mu A^2 \omega \sin 2\tau], \\ G_4(\tau) &= \frac{1}{\omega^2} (1 + 4K - \mu A^2 \omega \sin 2\tau). \end{aligned}$$

From the expressions of $G_2(\tau)$ and $G_4(\tau)$, the critical ranges of the coupling parameter K for which instability arises in the network can be determined. Thus, for a given α , instability will occur in the network for any value of the coupling parameter belonging to the union of the following domains

$$D^1 = \left(-\infty, -\frac{1}{2 + 4\alpha}\right),$$

$$D^2 = (-\infty, -0.250). \tag{7}$$

Any perturbed trajectory in those domains would lead the oscillators to continuously drift away from their original limit cycles because the restoring force turns out to be repelling and the cycle loses its attraction character. Consequently, Θ_2 , Θ_3 and Θ_4 will grow indefinitely, leading to the instability in the network. To further investigate on the stability analysis, we rewrite Eqs. (6) in a standard form by using the transformation

$$\Theta_k = \eta_k \exp(-\lambda\tau) \exp\left[-\frac{1}{2} \int F(\tau) d\tau\right]. \tag{8}$$

Thus, η_k satisfy the following set of independent Hill equations [27,28]

$$\ddot{\eta}_k + (a_{0k} + 2a_{1s} \sin 2\tau + 2a_{1c} \cos 2\tau + 2a_{2c} \cos 4\tau)\eta_k = 0, \quad 1 \leq k \leq 4, \tag{9}$$

where

$$a_{01} = \frac{1}{\omega^2} \left[1 - \frac{\mu^2}{4} \left(1 - \frac{A^2}{2} \right)^2 - \mu^2 \frac{A^4}{32} \right],$$

$$a_{02} = a_{03} = \frac{1}{\omega^2} \left[1 + (2 + 4\alpha)K - \frac{\mu^2}{4} \left(1 - \frac{A^2}{2} \right)^2 - \mu^2 \frac{A^4}{32} \right],$$

$$a_{04} = \frac{1}{\omega^2} \left[1 + 4K - \frac{\mu^2}{4} \left(1 - \frac{A^2}{2} \right)^2 - \mu^2 \frac{A^4}{32} \right],$$

$$a_{1s} = -\frac{\mu A^2}{4\omega}, \quad a_{1c} = \frac{\mu^2}{8\omega^2} \left(1 - \frac{A^2}{2} \right) A^2, \quad a_{2c} = -\frac{\mu^2 A^4}{64\omega^2}.$$

From Eqs. (9), the stability boundaries of the synchronization process are to be investigated around the main parametric resonances defined at $a_0 = n^2$ ($n = 1; 2$). According to the Floquet theory [27,28], η_k may decay to zero or grow to infinity, and then decide the behavior of the independent Fourier modes Θ_k whose velocities are defined as:

$$\eta_{2,3} = \frac{2 + 4\alpha}{\omega^2},$$

$$\eta_4 = \frac{4}{\omega^2}. \tag{10}$$

The stability of each mode Θ_k will depend on its speed to enter or leave the synchronization manifold. Thus, we need to determine the range of K for the synchronization process to be achieved. To that end, the Whittaker method [27] is used to discuss unstable solutions and we assume that at the n th unstable region, each solution of Eqs. (9) is defined as:

$$\eta_k = e^{\zeta_k \tau} \sin(n\tau - \rho), \tag{11}$$

with ζ_k being the characteristic exponents and ρ a parameter. Substituting Eqs. (11) into Eqs. (9) and equating the coefficient of $\cos n\tau$ and $\sin n\tau$ separately to zero, makes it to obtain the following characteristic exponents

$$\zeta_k^2 = -(a_{0k} + n^2) + \sqrt{4n^2 a_{0k} + a_{ns}^2 + a_{nc}^2}. \tag{12}$$

The synchronization process is stable when the Fourier modes Θ_k go to zero as time increases. So that, the real part of $-\lambda \pm \zeta_k$ should be negative. Since λ is real and positive, the stability condition is reduced to $\lambda^2 > \zeta_k^2$. Consequently, we have from Eqs. (8) that the synchronization process is stable under the conditions

$$I_{k,\alpha}^n = (a_{0k} - n^2)^2 + 2(a_{0k} + n^2)\lambda^2 + \lambda^4 - a_{ns}^2 - a_{nc}^2 > 0; \quad n = 1, 2. \tag{13}$$

The ranges of the coupling parameter K leading to stability of synchronized states are analytically determined based upon Eqs. (13). Investigations will be restricted around the first parametric resonance ($n = 1$) since for $n = 2$, the criterion (13) is always fulfilled. One can then utilize $I_{k,\alpha}^1$ to forecast the stability boundaries of synchronized states in the network. When $K = 0$, the system is uncoupled and the Fourier modes Θ_2 , Θ_3 and Θ_4 degenerate into Θ_1 which is stable since it remains bounded as t tends to infinity (see Fig. 3). However, as soon as $K \neq 0$, the stability boundaries become α dependent and this lead to two major coupling cases, namely identical and nonidentical coupling parameters configuration.

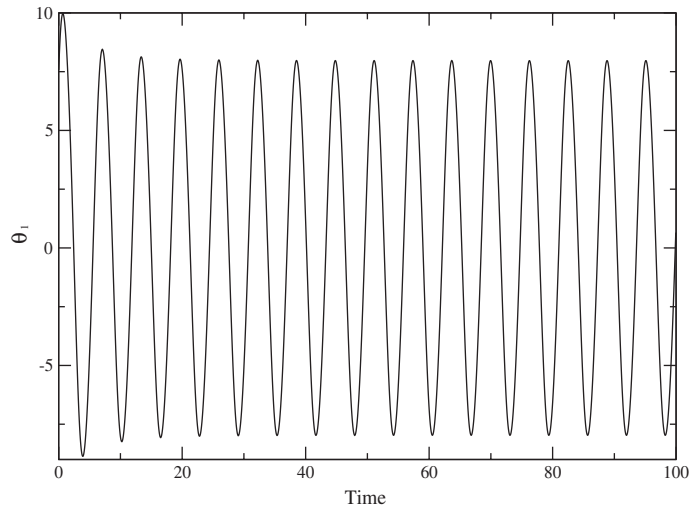


Fig. 3. A stable and bounded oscillation of the Fourier mode Θ_1 .

3.1.1. Stability boundaries for identical coupling parameters ($\alpha = 1$)

As K increases, our investigation shows that both $I_{2,1}^1$ and $I_{3,1}^1$ are positive for $K \in (-0.1666; -0.0004] \cup [0.0014; +\infty)$ while $I_{4,1}^1$ is positive for $K \in (-0.1666; -0.0006] \cup [0.002; +\infty)$. Thus, an intersection of these results allows the following three domains to be discerned:

$$\begin{aligned}
 D_{1a} &= (-0.1666, -0.0006] \cup [0.0020, +\infty), \\
 D_{2a} &= (-0.0006, -0.0004] \cup [0.0014, 0.0020), \\
 D_{3a} &= (-0.0004, 0) \cup (0, 0.0014).
 \end{aligned}$$

When $K \in D_{1a}$, the modes Θ_k ($k = 2, 3, 4$) are together in the stability domain and thus tend all to zero as the time increases. Consequently, all the four oscillators are phase-locked, leading to the following constraint:

$$x_1 = x_2 = x_3 = x_4. \tag{14}$$

In this case, all the oscillators are phase-locked and then display the same dynamics. Accordingly, a wave signal emitted emerges more powerful.

When $K \in D_{2a}$, the modes Θ_k ($k = 2, 3, 4$) enter into the instability domain and as a consequence, their state variables satisfy the following constraints:

$$\begin{aligned}
 x_1 &\neq x_3, \\
 x_3 &\neq x_4
 \end{aligned} \tag{15}$$

and

$$x_4 - x_3 + x_2 - x_1 \neq 0. \tag{16}$$

In this configuration, there is no synchronization in the network.

When $K \in D_{3a}$, the two degenerated modes and fastest modes Θ_2 and Θ_3 leave the stability domain and one have

$$\begin{aligned}
 x_1 &\equiv x_3, \\
 x_3 &\equiv x_4,
 \end{aligned} \tag{17}$$

while the slowest mode Θ_4 remains in the instability domain and thus, leading to the following criterion:

$$x_4 - x_3 + x_2 - x_1 \neq 0. \tag{18}$$

This state is sometimes referred to as *cluster synchronization* (clustering). Two clusters have emerged [Eqs. (17)] while there is no synchronization between them [Eqs. (18)]. This type of clustering is very useful since it corresponds for instance to a situation where two microwave oscillators are phase-locked one after the other one with possible implications in automation engineering, telecommunications, electronics commerce, robotics, transport technologies and many other areas [29].

3.1.2. Stability boundaries for nonidentical coupling parameters ($\alpha < 1, \alpha > 1$)

In this type of configuration, the coupling strength at both first and second range of interaction among oscillators is different [30]. Such situations are very common in several type of networks. It is for example the case of peri-glomerular cells in

the olfactory bulb, where stronger coupling might correspond to direct electrical connections and less stronger or weaker to indirect coupling via interpolated cells [31]. In each zone of α , three values will be considered for better capturing its influence on the synchronized states dynamics and their stability boundaries.

• **Case $\alpha < 1$**

In such a situation, the coupling strength between the first nearest neighbors has more influence compared to the one between non-nearest neighbors. The arbitrary values chosen here are $\alpha = 0.01$, $\alpha = 0.50$ and $\alpha = 0.90$.

For $\alpha = 0.01$, instability occurs in the network for $K \in (-\infty, -0.250)$. Around the first main parametric resonance, conditions (13) are satisfied for $I_{2,\alpha}^1(\alpha = 0.01) = I_{3,\alpha}^1(\alpha = 0.01)$ if $K \in (-0.250, -0.0010] \cup [0.0039, +\infty)$ and for $I_{4,\alpha}^1(\alpha = 0.01)$ if $K \in (-0.250, -0.00010] \cup [0.0026, +\infty)$. From these results the three following domains are derived

$$\begin{aligned} D_{1a,\alpha}(\alpha = 0.01) &= (-0.250, -0.0010] \cup [0.0039, +\infty), \\ D_{2a,\alpha}(\alpha = 0.01) &= (-0.0010, -0.0010] \cup [0.0026, 0.0039), \\ D_{3a,\alpha}(\alpha = 0.01) &= (-0.0010, 0) \cup (0, 0.0026), \end{aligned}$$

which stand for the regions of complete synchronization, Standard Correlated States (SCS) [32] and no synchronization respectively.

For $\alpha = 0.50$, the criteria $I_{2,\alpha}^1(\alpha = 0.50)$ and $I_{4,\alpha}^1(\alpha = 0.50)$ are realized when K belong to $K \in (-0.250, -0.0006] \cup [0.0020, +\infty)$ and $K \in (-0.250, -0.0010] \cup [0.0026, +\infty)$ respectively. In such a situation, four domains can be determined as follows

$$\begin{aligned} D_{1a,\alpha}(\alpha = 0.50) &= (-0.250, -0.0006] \cup [0.0026, +\infty), \\ D_{2a,\alpha}(\alpha = 0.50) &= (-0.0006, -0.00010], \\ D_{3a,\alpha}(\alpha = 0.50) &= (-0.0010, 0) \cup (0, 0.0020), \\ D_{4a,\alpha}(\alpha = 0.50) &= [0.0020, 0.00260). \end{aligned}$$

$D_{ka,\alpha}(\alpha = 0.50)$ ($k = 1, 2, 3$) correspond to regions of full synchronization, SCS and no synchronization respectively while $D_{4a,\alpha}(\alpha = 0.50)$ stands for domains of cluster synchronization.

For $\alpha = 0.90$, the range of instability is defined for $K \in (-\infty, -0.1875)$. Consequently, if $K \in (-0.1785, -0.0004] \cup [0.0014, +\infty)$ and $K \in (-0.1785, -0.0010] \cup [0.0026, +\infty)$, $I_{2,\alpha}^1(\alpha = 0.90)$ and $I_{4,\alpha}^1(\alpha = 0.90)$ are respectively satisfied and four domains can be determined and classified as follows:

$$\begin{aligned} D_{1a,\alpha}(\alpha = 0.90) &= (-0.1785, -0.0004] \cup [0.0026, +\infty), \\ D_{2a,\alpha}(\alpha = 0.90) &= (-0.0004, -0.00010], \\ D_{3a,\alpha}(\alpha = 0.90) &= (-0.0010, 0) \cup (0, 0.0014), \\ D_{4a,\alpha}(\alpha = 0.90) &= [0.0014, 0.00260), \end{aligned}$$

$D_{ka,\alpha}(\alpha = 0.90)$ ($k = 1, 2, 3, 4$) represent domains of full synchronization, SCS, no synchronization and clustering respectively.

It should be emphasized that when $\alpha < 1$, the number of dynamical states passes from three to four and as α increases, the range of the Standard Correlated States continuously decreases while ranges of *clustering* (cluster synchronization) begin to emerge.

• **Case $\alpha > 1$**

In such a configuration, the coupling strength between the non-nearest neighbors has more influence compared to the one between nearest neighbors. We have chosen the values of α to be 2, 6 and 10 and their corresponding domain of instability are $K \in (-\infty, -0.10)$, $K \in (-\infty, -0.03840)$ and $K \in (-\infty, -0.02380)$ respectively.

For $\alpha = 2$, $I_{2,\alpha}^1(\alpha = 2) > 0$ when $K \in (-0.10, -0.0003] \cup [0.0008, +\infty)$ while $I_{4,\alpha}^1(\alpha = 2) > 0$ if $K \in (-0.10, -0.00010] \cup [0.0026, +\infty)$. Consequently, the domains of complete synchronization, Standard Correlated States, no synchronization and clustering are respectively defined as:

$$\begin{aligned} D_{1a,\alpha}(\alpha = 2) &= (-0.10, -0.0003] \cup [0.0026, +\infty), \\ D_{2a,\alpha}(\alpha = 2) &= (-0.0003, -0.00010], \\ D_{3a,\alpha}(\alpha = 2) &= (-0.0010, 0) \cup (0, 0.0008), \\ D_{4a,\alpha}(\alpha = 2) &= [0.0008, 0.00250]. \end{aligned}$$

For $\alpha = 6$, the criteria $I_{2,\alpha}^1(\alpha = 6)$ and $I_{4,\alpha}^1(\alpha = 6)$ are respectively satisfied for $K \in (-0.0384, -0.0001] \cup [0.0004, +\infty)$ and $K \in (-0.0384, -0.00010] \cup [0.0026, +\infty)$. Thus, the states of full synchronization, no synchronization and clustering are defined respectively as:

$$D_{1a,\alpha}(\alpha = 6) = (-0.0384, -0.0001] \cup [0.0026, +\infty),$$

$$D_{2a,\alpha}(\alpha = 6) = (-0.0010, 0) \cup (0, 0.0004),$$

$$D_{3a,\alpha}(\alpha = 6) = [0.0004, 0.0026).$$

For $\alpha = 10$, the criteria $I_{2,\alpha}^1(\alpha = 10)$ and $I_{4,\alpha}^1(\alpha = 10)$ are satisfied respectively when $K \in (-0.0238, -0.0001] \cup [0.0002, +\infty)$ and when $K \in (-0.0238, -0.00010] \cup [0.0026, +\infty)$. From where, the following intervals

$$D_{1a,\alpha}(\alpha = 10) = (-0.0238, -0.0001] \cup [0.0026, +\infty),$$

$$D_{2a,\alpha}(\alpha = 10) = (-0.0010, 0) \cup (0, 0.0002),$$

$$D_{3a,\alpha}(\alpha = 10) = [0.0002, 0.0025),$$

stand respectively for domains of full synchronization, no synchronization and cluster synchronization.

3.2. Results of numerical simulations

Numerical simulations are carried out to support the accuracy and complement the findings of analytical investigations. Thus, a fourth-order Runge–Kutta algorithm with a time step $\Delta t = 10^{-2}$ and the following initial conditions $(x_1(0); x_1(0)) = (1.0; 1.0)$, $(x_2(0); x_2(0)) = (1.5; 1.5)$, $(x_3(0); x_3(0)) = (2.0; 2.0)$ and $(x_4(0); x_4(0)) = (3.0; 3.0)$ are used. In the cases of non-identical and identical coupling parameters, the network is considered in phase synchronization when each mode Θ_k vanishes with the precision 10^{-4} .

• Case $\alpha = 1$

The corresponding time series of Θ_k ($k = 2, 3, 4$) for synchronization, no synchronization and instability are plotted as shown in Fig. 4. for values of K in each area D_{ka} ($k = 1, 2, 3$),

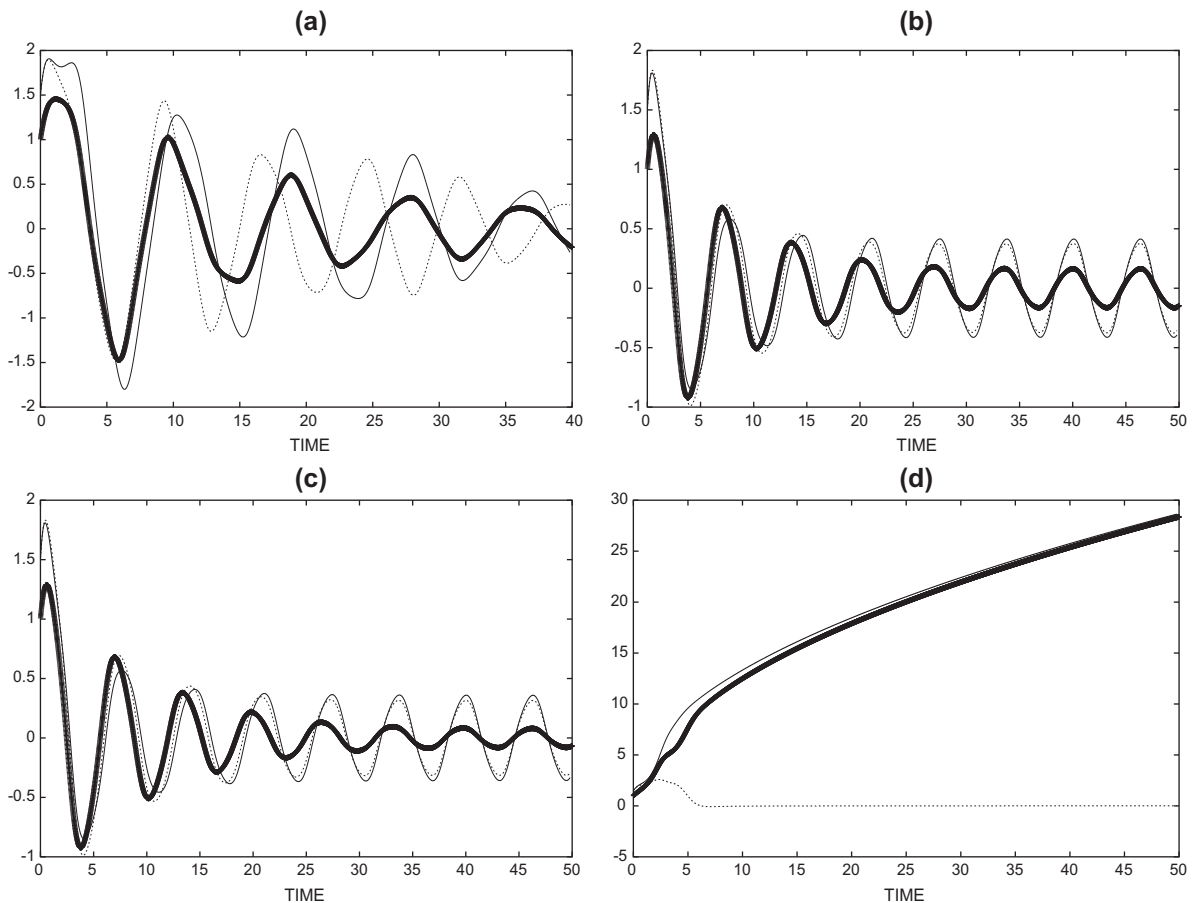


Fig. 4. Temporal variation of the Fourier modes Θ_k for $\mu = 0.1$: (a) $K = -0.08$, (b) $K = -0.0002$, (c) $K = 0.0015$, (d) $K = -0.17$; Θ_2 (lines), Θ_3 (dashed lines), Θ_4 (points).

The numerical simulation of Eqs. (2) reveal that the network is completely synchronized for $K \in [-0.1474; -0.0010] \cup [0.0018; +\infty)$ where $\Theta_k = 0$. There is a lack of synchronization in the system for $K \in (-0.0006, 0) \cup (0, 0.0013)$. Such a lack happens because $\Theta_j \neq 0$. Clusters occur for $K \in [-0.0009, -0.0006] \cup [0.0013, 0.0017]$ where $\Theta_2 = \Theta_3 = 0$ while $\Theta_4 \neq 0$. This clustering corresponds to the state where $x_2 = x_4$ and $x_1 = x_3$ with $x_4 - x_3 + x_2 - x_1 \neq 0$. The numerical simulations also reveal the existence of the Standard Correlated States for $K \in [-0.1666; -0.1474]$. For this last oscillatory pattern, the faster mode is $\Theta_4 = 0$ while the slower and degenerated modes are greater than the given precision and therefore remain in the instability domain. Overall, there is a quite good agreement between the results of the analytical and the numerical investigations.

• Case $\alpha < 1$

For $\alpha = 0.01$, complete synchronization takes place for K belonging to $D_{1n,\alpha}(\alpha = 0.01) = [-0.2363, -0.0017] \cup [0.0037, +\infty)$ while the SCS ($\Theta_2 \neq \Theta_3 \neq 0, \Theta_4 = 0$) arises if $K \in D_{2n,\alpha}(\alpha = 0.01) = [-0.0010, -0.00090] \cup [0.0029, 0.0036]$ and no synchronization for $K \in D_{3n,\alpha}(\alpha = 0.01) = (-0.00090, 0) \cup (0, 0.0028]$. Apart these dynamical states forecasted

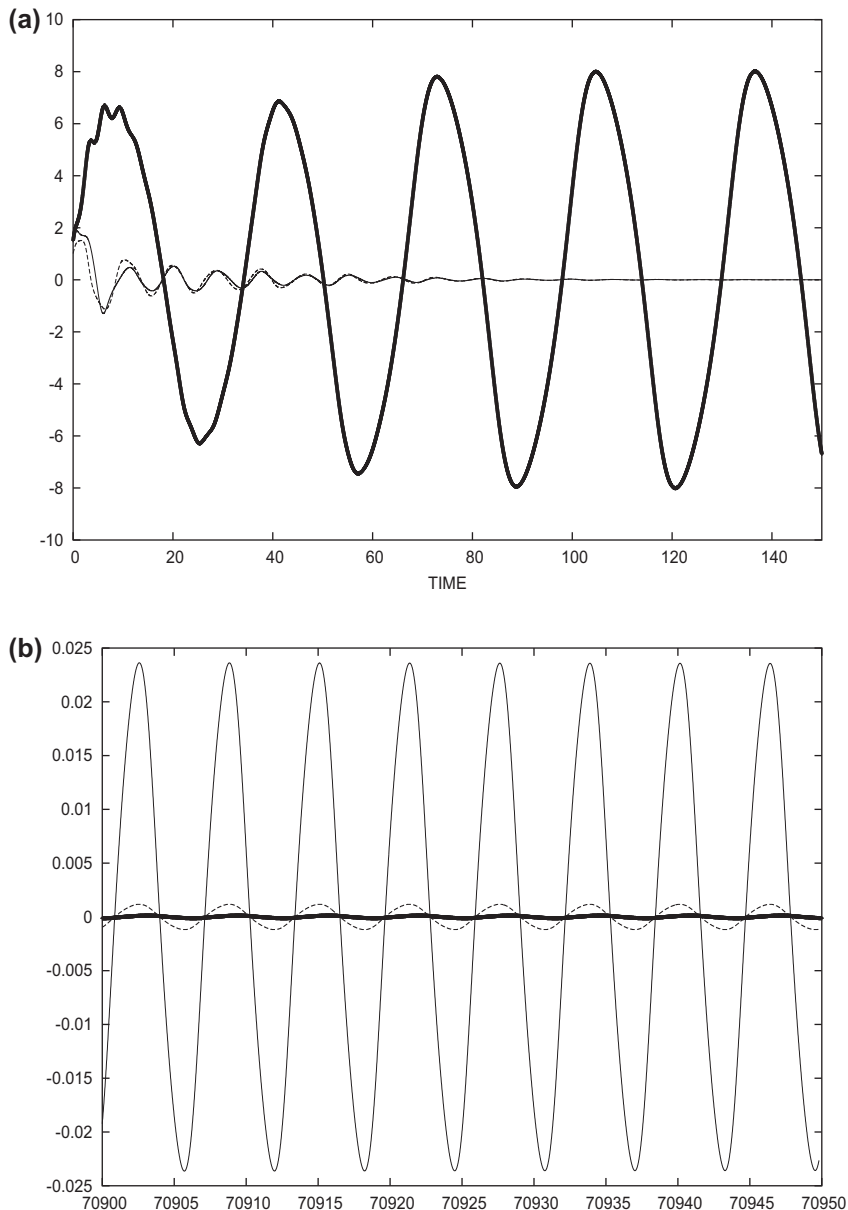


Fig. 5. Temporal variation of the Fourier modes Θ_k with $\mu = 0.10$ for $\alpha = 0.01$. (a): $K = -0.240$, (b): $K = -0.0014$. Θ_2 (lines), Θ_3 (dashed lines), Θ_4 (points).

analytically, clusters also appear for $K \in [-0.250, -0.2364]$ while the Cluster Correlated States (CCS) for which $\Theta_2 \neq 0$, $\Theta_3 = 0$ and $\Theta_4 = 0$ emerge in the range of K defined as $[-0.00160, -0.00110]$.

As α continuously increases, there is no significant change on the nature of dynamical states occurring in the network and their stability boundaries until $\alpha = 0.50$ for which full synchronization is now defined for $K \in D_{1n,\alpha}(\alpha = 0.50) = [-0.2294, -0.0009] \cup [0.0020, +\infty)$ while the SCS emerges for $K \in D_{2n,\alpha}(\alpha = 0.50) = [-0.2497, -0.2494] \cup [-0.2303, -0.2295]$.

No synchronization is observed if $K \in D_{3n,\alpha}(\alpha = 0.50) = [-0.250, -0.2498] \cup [-0.2493, -0.2304] \cup (-0.0005, 0) \cup (0, 0.0020)$. One should notice the non appearance of clustering analytically predicted for $\alpha = 0.50$ but instead, the occurrence Clusters Correlated States for $K \in (0.0017, 0.0020)$.

But, when $\alpha = 0.90$, all dynamical states predicted analytically are observed during numerical simulations and classified as follows: For $K \in D_{1n,\alpha}(\alpha = 0.90) = (-0.1580, -0.0010) \cup (0.0017, +\infty)$, synchronous states are observed while the SCS occur for $K \in D_{2n,\alpha}(\alpha = 0.90) = [-0.1785, -0.1580]$. Instability is displayed for $K \in D_{3n,\alpha}(\alpha = 0.90) = (-0.0006, 0) \cup (0, 0.0012)$ while clusters exist for $K \in D_{4n,\alpha}(\alpha = 0.90) = (-0.0011, -0.0005) \cup [0.0014, 0.0017]$.

Overall, there is a good agreement between results of analytical and numerical investigations.

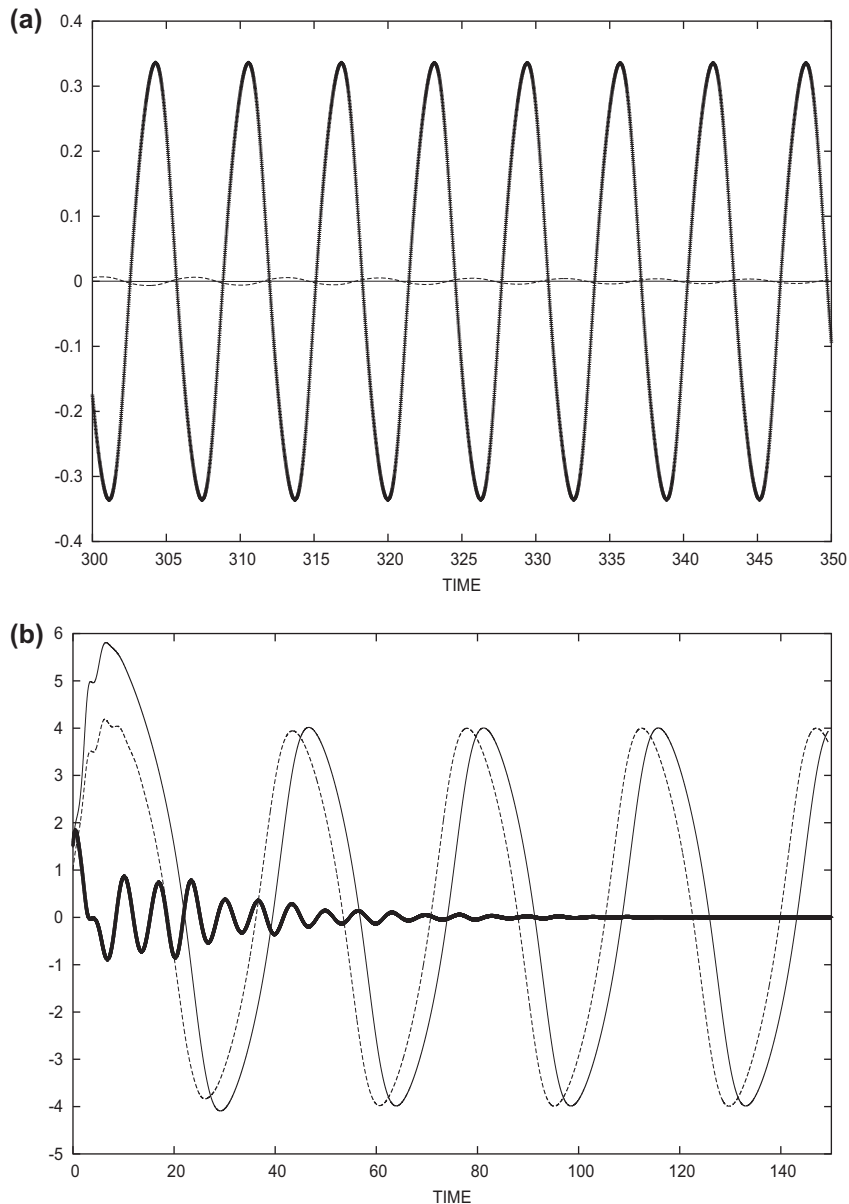


Fig. 6. Temporal variation of the Fourier modes Θ_k with $\mu = 0.10$ for $\alpha = 10$. (a): $K = 0.0018$, (b): $K = -0.0230$. Θ_2 (lines), Θ_3 (dashed lines), Θ_4 (points).

• Case $\alpha > 1$

For $\alpha = 2$, full synchronization occurs if $K \in D_{1n,\alpha}(\alpha = 2) = (-0.0884, -0.00080) \cup (0.0018, +\infty)$ and the SCS are observed for $K \in D_{2n,\alpha}(\alpha = 2) = [-0.10, -0.0884]$. Instability appears for $K \in D_{3n,\alpha}(\alpha = 2) = [-0.0002, 0) \cup (0, 0.0006]$ while clusters are defined for $K \in D_{4n,\alpha}(\alpha = 2) = [-0.0008, -0.0005] \cup [0.0009, 0.0018]$.

For $\alpha = 6$, the domain of complete synchronization, no synchronization, clustering and SCS obtained are respectively $D_{1n,\alpha}(\alpha = 6), D_{2n,\alpha}(\alpha = 6), D_{3n,\alpha}(\alpha = 6), D_{4n,\alpha}(\alpha = 6)$ and defined as:

$$\begin{aligned} D_{1n,\alpha}(\alpha = 6) &= (-0.0343, -0.00070) \cup (0.0019, +\infty), \\ D_{2n,\alpha}(\alpha = 6) &= (-0.0001, 0) \cup (0, 0.0003), \\ D_{3n,\alpha}(\alpha = 6) &= [-0.00070, -0.00020] \cup [0.00030, 0.00196], \\ D_{4n,\alpha}(\alpha = 6) &= [-0.0384, -0.0343]. \end{aligned}$$

For $\alpha = 10$, synchronous motions are found in the ring for $K \in D_{1n,\alpha}(\alpha = 10) = (-0.0216, -0.00070) \cup (0.0019, +\infty)$. No synchronization is observed for $K \in D_{2n,\alpha}(\alpha = 10) = (-0.0001, 0) \cup (0, 0.0002]$ while the clusters and the SCS are observed for $K \in D_{3n,\alpha}(\alpha = 10) = [-0.0007, -0.0001] \cup (0.0002, 0.0020)$ and $K \in D_{4n,\alpha}(\alpha = 10) = (-0.0001, 0) \cup (0, 0.0002]$. In this case also, there is a overall good agreement between analytical and numerical results in spite of some little discrepancies observed. The time histories of cluster synchronization and Standard Correlated States are shown in Figs. 5 and 6 respectively for $\alpha = 0.01$ and $\alpha = 10$. Figs. 5(a) and 6(a) show the time series of cluster synchronization while Figs. 5(b) and 6(b) display the SCS.

4. Influence of a locally injected signal

4.1. Analytical survey

In order to consider the effects of undesirable parasite coupling or external perturbation, an external periodic signal is locally injected in the network. Thus, the dynamics of the network in this representation is described by the following equations:

$$\begin{aligned} \ddot{x}_1 - \mu(1 - x_1^2)\dot{x}_1 + x_1 &= K[x_2 + 2\alpha x_3 + x_4 - 2(\alpha + 1)x_1] - \Gamma(x_1 - x_c), \\ \ddot{x}_l - \mu(1 - x_l^2)\dot{x}_l + x_l &= K[x_{l+1} + 2\alpha x_{l+2} + x_{l-1} - 2(\alpha + 1)x_l], \quad 2 \leq l \leq 4, \end{aligned} \tag{19}$$

where x_c stands for the dynamics of the external oscillator and also plays the role of the command signal while Γ is the local injection strength. Throughout this survey, we take x_c as the periodic solution of a van der Pol equation. Thus, the first order perturbation equations for the stability analysis may now be written as:

$$\begin{aligned} \ddot{\zeta}_1 - \mu(1 - x_0^2)\dot{\zeta}_1 + [1 + 2K(1 + \alpha) + 2\mu x_0 \dot{x}_0]\zeta_1 &= K(\zeta_2 + 2\alpha\zeta_3 + \zeta_4) - \Gamma\zeta_1, \\ \ddot{\zeta}_l - \mu(1 - x_0^2)\dot{\zeta}_l + [1 + 2K(1 + \alpha) + 2\mu x_0 \dot{x}_0]\zeta_l &= K(\zeta_{l+1} + 2\alpha\zeta_{l+2} + \zeta_{l-1}), \end{aligned} \tag{20}$$

with the deviation $\zeta_k = x_k - x_c$.

Eqs. (20) can also be rewritten as the following set of coupled Hill's equations:

$$\begin{aligned} \ddot{\varepsilon}_1 + (a_{01} + 2a_{1s} \sin 2\tau + 2a_{1c} \cos 2\tau + 2a_{2c} \cos 4\tau)\varepsilon_1 &= \frac{1}{\omega^2} [K(\varepsilon_2 + 2\varepsilon_3 - 4\varepsilon_1 + \varepsilon_4) - \Gamma\varepsilon_1], \\ \ddot{\varepsilon}_l + (a_{01} + 2a_{1s} \sin 2\tau + 2a_{1c} \cos 2\tau + 2a_{2c} \cos 4\tau)\varepsilon_l &= \frac{1}{\omega^2} [K(\varepsilon_{l+1} + 2\varepsilon_{l+2} - 4\varepsilon_l + \varepsilon_{l-1})], \end{aligned} \tag{21}$$

where

$$\zeta_k = \varepsilon_k \exp(-\lambda\tau) \exp\left[-\frac{1}{2} \int F(\tau) d\tau\right], \quad 1 \leq k \leq 4 \tag{22}$$

In order to investigate the stability of the process around the parametric resonances, we assume that each solution of Eqs. (21) is defined as follows:

$$\varepsilon_k = C_k e^{S\tau} \sin(n\tau - \sigma), \tag{23}$$

where S represents a characteristic exponent while C_k and σ are arbitrary constants. Substituting the solutions (23) into Eqs. (21) and equating the coefficients of $\sin n\tau$ and $\cos n\tau$ separately to zero gives us the following set of algebraic equations in C_k :

$$\left\{ [S^2 + \aleph_n(\alpha)] \cos \sigma + (2nS - a_{ns}) \sin \sigma \right\} C_1 - \frac{K}{\omega^2} \cos \sigma C_2 - \frac{2\alpha K}{\omega^2} \cos \sigma C_3 - \frac{K}{\omega^2} \cos \sigma C_4 = 0,$$

$$\begin{aligned}
 & \left\{ (2nS + a_{ns}) \cos \sigma - [S^2 + \Xi_n(\alpha)] \sin \sigma \right\} C_1 + \frac{K}{\omega^2} \sin \sigma C_2 + \frac{2\alpha K}{\omega^2} \sin \sigma C_3 + \frac{K}{\omega^2} \sin \sigma C_4 = 0, \\
 & -\frac{K}{\omega^2} \cos \sigma C_1 + \left\{ [S^2 + \Upsilon_n(\alpha)] \cos \sigma + (2nS - a_{ns}) \sin \sigma \right\} C_2 - \frac{K}{\omega^2} \cos \sigma C_3 - \frac{2\alpha K}{\omega^2} \cos \sigma C_4 = 0, \\
 & \frac{K}{\omega^2} \sin \sigma C_1 + \left\{ (2nS + a_{ns}) \cos \sigma - [S^2 + \Psi_n(\alpha)] \sin \sigma \right\} C_2 + \frac{K}{\omega^2} \sin \sigma C_3 + \frac{2\alpha K}{\omega^2} \sin \sigma C_4 = 0, \\
 & -\frac{2\alpha K}{\omega^2} \cos \sigma C_1 - \frac{K}{\omega^2} \cos \sigma C_2 + \left\{ [S^2 + \Upsilon_n(\alpha)] \cos \sigma + (2nS - a_{ns}) \sin \sigma \right\} C_3 - \frac{K}{\omega^2} \cos \sigma C_4 = 0, \\
 & \frac{2\alpha K}{\omega^2} \sin \sigma C_1 + \frac{K}{\omega^2} \sin \sigma C_2 + \left\{ (2nS + a_{ns}) \cos \sigma - [S^2 + \Psi_n(\alpha)] \sin \sigma \right\} C_3 + \frac{K}{\omega^2} \sin \sigma C_4 = 0, \\
 & -\frac{K}{\omega^2} \cos \sigma C_1 - \frac{2\alpha K}{\omega^2} \cos \sigma C_2 - \frac{K}{\omega^2} \cos \sigma C_3 + \left\{ [S^2 + \Upsilon_n(\alpha)] \cos \sigma + (2nS - a_{ns}) \sin \sigma \right\} C_4 = 0, \\
 & \frac{K}{\omega^2} \sin \sigma C_1 + \frac{2\alpha K}{\omega^2} \sin \sigma C_2 + \frac{K}{\omega^2} \sin \sigma C_3 + \left\{ (2nS + a_{ns}) \cos \sigma - [S^2 + \Psi_n(\alpha)] \right\} \Psi_4 = 0.
 \end{aligned} \tag{24}$$

When C_k and σ are discarded in Eqs. (24), the characteristic equation for S is defined by

$$\Delta_{n,\alpha}(S) \equiv \begin{vmatrix} \Delta_{11} & \Delta_{12} & \Delta_{13} & 0 & \Delta_{15} & 0 & \Delta_{17} & 0 \\ \Delta_{21} & \Delta_{22} & 0 & \Delta_{24} & 0 & \Delta_{26} & 0 & \Delta_{28} \\ \Delta_{31} & 0 & \Delta_{33} & \Delta_{34} & \Delta_{35} & 0 & \Delta_{37} & 0 \\ 0 & \Delta_{42} & \Delta_{43} & \Delta_{44} & 0 & \Delta_{46} & 0 & \Delta_{48} \\ \Delta_{51} & 0 & \Delta_{53} & 0 & \Delta_{55} & \Delta_{56} & \Delta_{57} & 0 \\ 0 & \Delta_{62} & 0 & \Delta_{64} & \Delta_{65} & \Delta_{66} & 0 & \Delta_{68} \\ \Delta_{71} & 0 & \Delta_{73} & 0 & \Delta_{75} & 0 & \Delta_{77} & \Delta_{78} \\ 0 & \Delta_{82} & 0 & \Delta_{84} & 0 & \Delta_{86} & \Delta_{87} & \Delta_{88} \end{vmatrix} = 0; \quad n = 1, 2, \tag{25}$$

where

$$\begin{aligned}
 \Delta_{11} &= S^2 + \aleph_n(\alpha), & \Delta_{22} &= -(S^2 + \Xi_n(\alpha)), & \Delta_{33} &= \Delta_{55} = \Delta_{77} = S^2 + \Upsilon_n(\alpha), \\
 \Delta_{44} &= \Delta_{66} = \Delta_{88} = -(S^2 + \Psi_n), & \Delta_{12} &= \Delta_{34} = \Delta_{56} = \Delta_{78} = 2nS - a_{ns}, \\
 \Delta_{21} &= \Delta_{43} = \Delta_{65} = \Delta_{87} = 2nS + a_{ns}, \\
 \Delta_{13} &= \Delta_{31} = \Delta_{17} = \Delta_{71} = \Delta_{35} = \Delta_{53} = \Delta_{57} = \Delta_{75} = -\frac{K}{\omega^2}, \\
 \Delta_{24} &= \Delta_{42} = \Delta_{28} = \Delta_{82} = \Delta_{46} = \Delta_{64} = \Delta_{68} = \Delta_{86} = \frac{K}{\omega^2}, \\
 \Delta_{15} &= \Delta_{51} = \Delta_{37} = \Delta_{73} = -\frac{2\alpha K}{\omega^2}, & \Delta_{26} &= \Delta_{62} = \Delta_{48} = \Delta_{84} = \frac{2\alpha K}{\omega^2} \\
 \delta &= \frac{2(\alpha + 1)K + \Gamma}{\omega^2}, & \aleph_n(\alpha) &= a_{01} + \delta - n^2 - a_{nc}, & \Xi_n(\alpha) &= a_{01} + \delta - n^2 + a_{nc}, \\
 \Upsilon_n(\alpha) &= a_{01} + \frac{2(\alpha + 1)K}{\omega^2} - n^2 - a_{nc}, & \Psi_n(\alpha) &= a_{01} + \frac{2(\alpha + 1)K}{\omega^2} - n^2 + a_{nc},
 \end{aligned}$$

with $n = 1$ for $\Delta_1(S)$ and $n = 2$ for $\Delta_2(S)$ (see Eq. (25)).

Since the stability condition is given by $\lambda^2 - S^2 > 0$ when we assume that $\lambda > 0$, we have at the boundary of the n th unstable domain

$$\Delta_{n,\alpha}(\lambda) = 0. \tag{26}$$

The stability analysis here is reduced around the first unstable area because $\Delta_{2,\alpha}(\lambda) > 0$ remain positive for all values of the coupling parameter K . Therefore, the process will be considered stable if $\Delta_{1,\alpha}(\lambda) > 0$ and unstable otherwise. Thus, to analyze the modulation of stability boundaries by the local injection strength, Eq. (26) is solved for $\alpha = 1$, $\alpha < 1$ and $\alpha > 1$.

4.1.1. Stability boundaries for identical coupling parameters ($\alpha = 1$)

Two main ranges of stability boundaries are found around $\Delta_1(S)$ as Γ is varied. The first one is defined as $0 < \Gamma < 1.20$ where the range of stability domain in the network is a function of the local injection strength Γ . For instance, when $\Gamma = 0.03$, synchronized states are found in the ring for $K \in [-0.1009, -0.0015] \cup [0.0014, 0.0016]$. But when $\Gamma = 0.05$, a phase synchronization process is achieved for $K \in (-0.1666, -0.0016] \cup [0.0014, 0.0016] \cup [0.0139, +\infty)$ and for

$K \in (-0.1666, -0.0016] \cup [0.0014, 0.0016] \cup [0.0087, +\infty)$ when $\Gamma = 0.09$. In the second range ($\Gamma > 1.20$), the stability boundaries of phase synchronization remain unchanged and are defined for $K \in (-0.1666, -0.0018] \cup [0.0014, 0.0016] \cup [0.0062, +\infty)$.

4.1.2. Stability boundaries for nonidentical coupling parameters ($\alpha < 1, \alpha > 1$)

In both ranges of α , two main ranges are found as Γ varies. Generally, stability boundaries are dependent on Γ in the first range. On the other hand, stability boundaries remain unchanged in the second range for any value of the local injection strength. Moreover, the size of that first range differs as α increases.

When $\alpha < 1$, the first range for $\alpha = 0.01, \alpha = 0.5$ and $\alpha = 0.9$ are defined as $0 < \Gamma \leq 0.5, 0 < \Gamma \leq 0.75$ and $0 < \Gamma \leq 0.80$ respectively. But when $\alpha > 1$, the first range for $\alpha = 2, \alpha = 6$ and $\alpha = 10$ is respectively defined as $0 < \Gamma \leq 0.5, 0 < \Gamma \leq 0.30$ and $0 < \Gamma \leq 0.24$. The threshold of the local injection strength from which stability boundaries of main dynamical states remain unchanged is inversely proportional to α when $\alpha > 1$ but proportional to α for $\alpha < 1$. In other words, when $\alpha \in (0, 1)$, the threshold of the local injection strength at which the stability boundaries of the synchronization dynamics remain practically unchanged, increases. On the other hand for $\alpha \in (1, +\infty)$, that threshold decreases as Γ increases. Therefore, α can be viewed as a modulatory parameter of the local injection threshold.

4.2. Results of numerical simulations

The validity of the analytical findings is checked by solving Eqs. (19) numerically for identical and nonidentical coupling parameters. In both coupling configurations, two oscillators u and v are synchronized if the distance of their phase trajectories

$$d_{uv} = |x_u - x_v| < h, \tag{27}$$

where $h = 10^{-4}$ is the precision. Thus, synchronization among all the oscillators is achieved if the total separation of all pairs of trajectories (TS) is smaller than the precision, namely

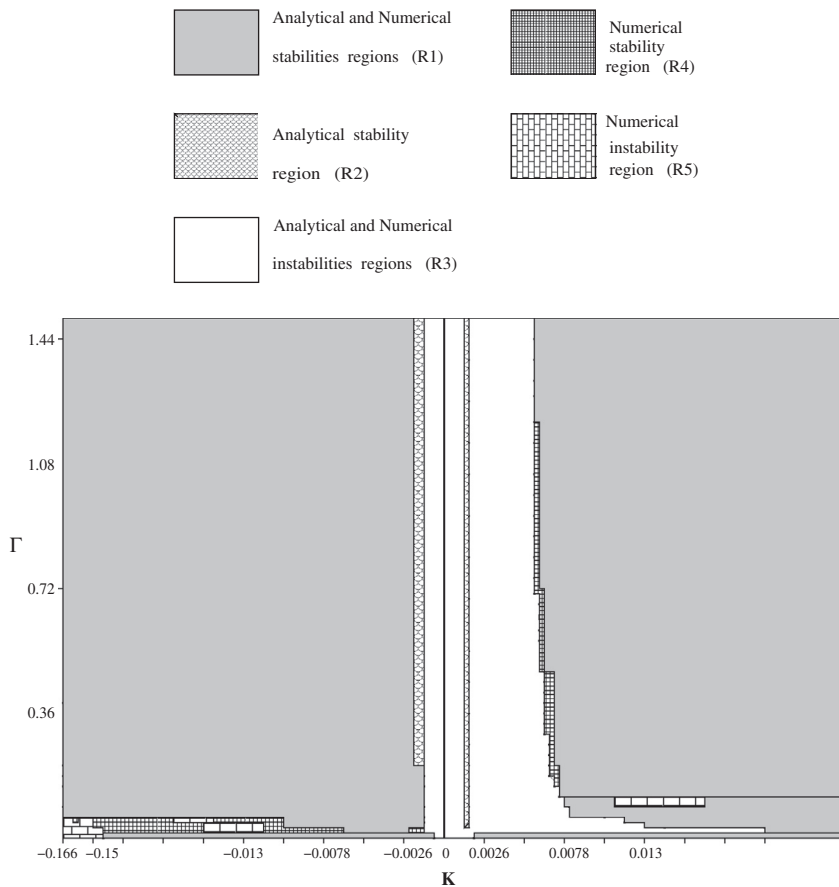


Fig. 7. Stability map showing the resulting synchronized states when both the first and second nearest neighbors are considered for identical coupling parameters.

$$TS = \sum_{\text{pairs}(uv)} d_{uv} < h. \tag{28}$$

For higher accuracy (with a smaller h), the computational time has been extended to 10^5 .

• Case of identical coupling parameters

A chart reporting possible synchronized states with their corresponding stability boundaries is constructed in the (K, Γ) plane as shown in Fig. 7. by combining results of numerical simulations of Eqs. (19) and the analytical findings. Fig. 7 is composed of five different regions: (R1), (R2), (R3), (R4) and (R5). (R1) occurs from intersection between the analytical and numerical stabilities areas while (R3) represents the common solutions obtained from the numerical and analytical instability domains. (R2) is the stability area forecasted analytically but absent from numerical simulations. (R4) and (R5) are respectively the stability and the instability domains obtained numerically but not predicted analytically. Discrepancy between the analytical and the numerical results decreases as Γ increases. For instance, synchronization is numerically achieved when $K \in [-0.1488, -0.0261] \cup [-0.0113, -0.0020] \cup [0.0337, +\infty)$ for $\Gamma = 0.03$ and when $K \in [-0.1666, -0.0013] \cup [0.0081, 0.0112] \cup [0.0161, +\infty)$ for $\Gamma = 0.09$. Clustering occurs in (R5) since a full synchronization requires all clusters to be synchronized among them. For example, when $\Gamma = 0.02$, six clusters ($x_1 = x_2; x_1 = x_3; x_1 = x_4; x_2 = x_3; x_2 = x_4; x_3 = x_4$) exist for K defined as $K \in [-0.135; -0.033]$ while for $\Gamma = 0.05$, there are three clusters ($x_2 = x_3; x_2 = x_4; x_3 = x_4$) when $K \in [0.007; 0.0096]$. These clusters which mostly occur for small values of the local injection strength progressively disappear by becoming synchronized as Γ increases. $\Gamma = 1.20$ is the critical value above which stability boundaries of synchronized states remain unchanged when both the first and second nearest neighbors coupling are taken into account. This critical value is lower than the one reported ($\Gamma = 1.44$) when only first neighbors coupling is considered [16]. Therefore, the range of interaction in a network not only modulates synchronized states with their stability boundaries, but also the energy threshold needed to be injected in the system in order to observe a steadiness of stability boundaries.

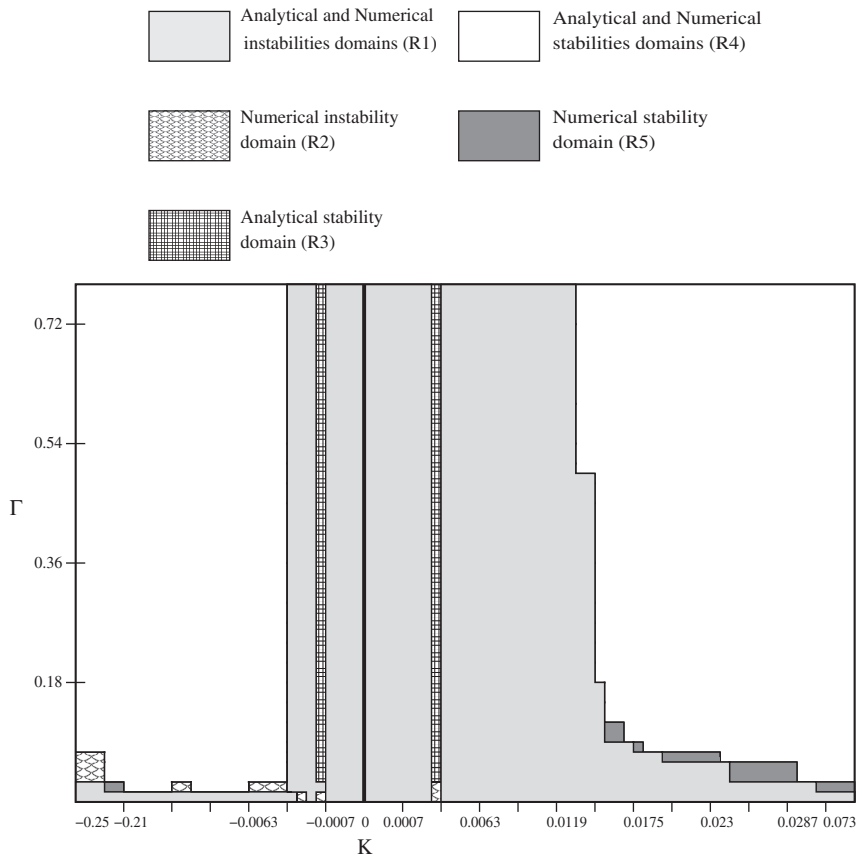


Fig. 8. Stability map showing the resulting synchronized states when both the first and second nearest neighbors are considered for non-identical coupling parameters ($\alpha = 0.01$).

• Case of nonidentical coupling parameters

For nonidentical coupling parameters, the accuracy of the analytical results predicted by Eq. (26) is solved for $\alpha < 1$ and $\alpha > 1$ (namely $\alpha = 0.01, \alpha = 0.50, \alpha = 0.90, \alpha = 2, \alpha = 6$ and $\alpha = 10$). A very good agreement is obtained between the results of numerical and analytical investigations, both for $\alpha < 1$ and $\alpha > 1$. To illustrate such situations, we have constructed two stability charts showing the resulting synchronized states for $\alpha = 0.01$ and $\alpha = 10$ as shown in Fig. 8 and Fig. 9 respectively.

In both zones of α , two main ranges of Γ emerge. Here as well, stability boundaries in the first range vary for different values of the local injection strength while in the second range, those boundaries remain the same despite increasing values of Γ . For example, when $\alpha = 0.01$, the synchronization is effective if $K \in [-0.2382, -0.0547] \cup [-0.0234, -0.0067] \cup [0.0726, +\infty)$ for $\Gamma = 0.03$. This domain changes for $\Gamma = 0.18$ and occurs when $K \in (-0.25, -0.0041] \cup [0.0154, +\infty)$. But as soon as $\Gamma > 0.50$, the synchronization process is achieved for $K \in (-0.25, -0.0042] \cup [0.0133, +\infty)$.

On the other hand for $\alpha = 10$, synchronized states are displayed for $K \in [-0.0221, -0.0191] \cup [-0.0063, -0.0017] \cup [0.0218, +\infty)$ if $\Gamma = 0.03$ while when $\Gamma = 0.09$, those states occur for $K \in (-0.0238, -0.0013) \cup [0.0060, +\infty)$. Very little changes are noticed on these stability boundaries for $\Gamma > 0.24$ and they are defined as being $(-0.0238, -0.0014] \cup [0.0044, +\infty)$.

In an attempt to explore the limits of the stability regions, a small amount of noise is added to the locally injected signal in the network. Under this circumstance, the network is governed by the following equations.

$$\begin{aligned} \ddot{x}_1 - \mu(1 - x_1^2)\dot{x}_1 + x_1 &= K[x_2 + 2\alpha x_3 + x_4 - 2(\alpha + 1)x_1] - \Gamma(x_1 - x_c) + \xi(t), \\ \ddot{x}_l - \mu(1 - x_l^2)\dot{x}_l + x_l &= K[x_{l+1} + 2\alpha x_{l+2} + x_{l-1} - 2(\alpha + 1)x_l], \quad 2 \leq l \leq 4. \end{aligned} \tag{29}$$

The stochastic term $\xi(t)$ is a Gaussian white noise of zero mean (i.e. $\langle \xi(t) \rangle = 0$ and $\langle \xi(t)\xi(t') \rangle = 0$) and correlation $\langle \xi(t)\xi(t') \rangle = 2D\delta(t - t')$ with D being the intensity of the noise. From the numerical simulations of the above equations and utilizing the synchronization criterion defined by Eq. (28), Figs. 10 and 11 are obtained for both identical and

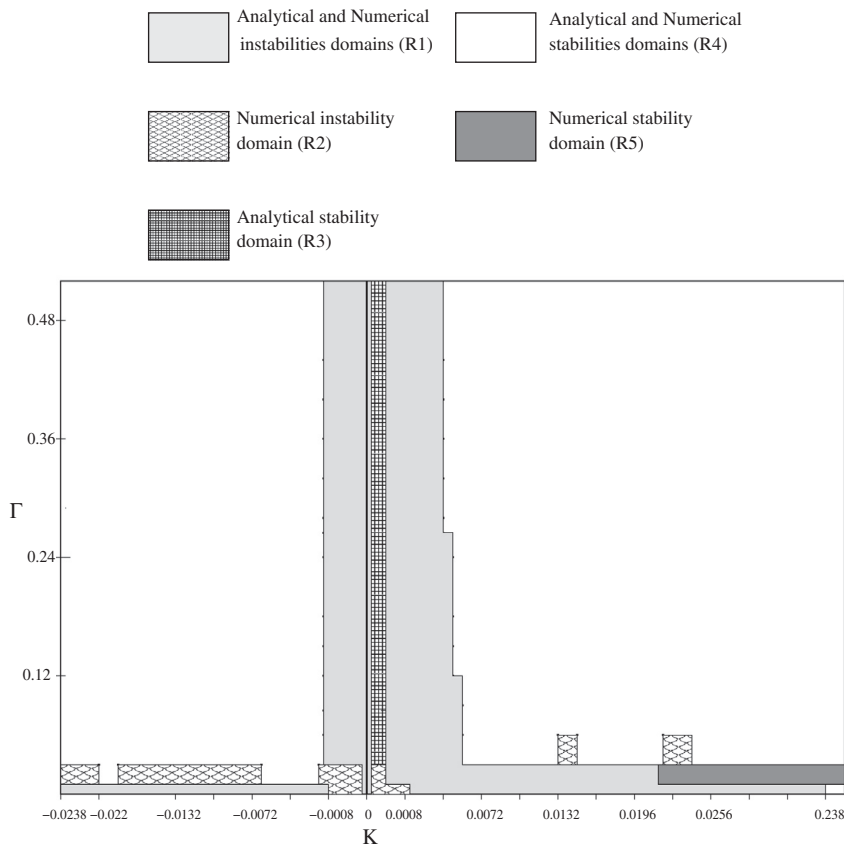


Fig. 9. Stability map showing the resulting synchronized states when both the first and second nearest neighbors are considered for non-identical coupling parameters ($\alpha = 10$).

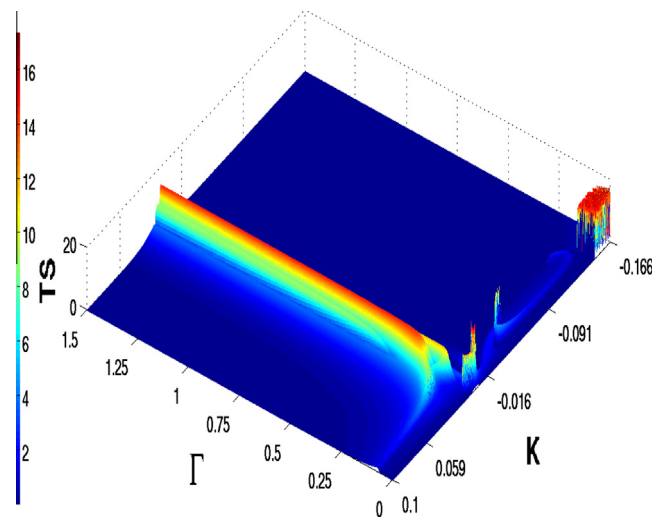


Fig. 10. Effects of a small Gaussian white noise on the stability map when both the first and second nearest neighbors are considered for identical coupling parameters ($\alpha = 1; D = 0.02$).

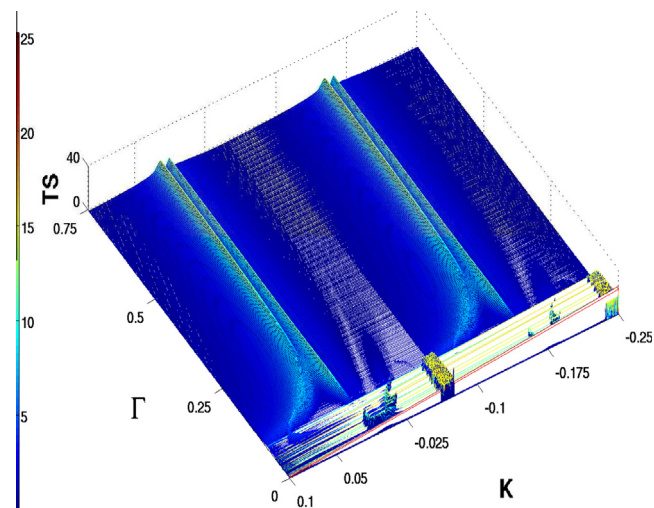


Fig. 11. Effects of a small Gaussian white noise on the stability map when both the first and second nearest neighbors are considered for non-identical coupling parameters ($\alpha = 0.01; D = 0.02$).

non-identical coupling parameters respectively. In the case of identical coupling parameters, the stability boundaries of synchronization states are merely affected by local injection of a small amount of noise while the most remarkable change is related to the critical value of Γ above which the stability boundaries remain unchanged for admissible values of coupling parameters. In fact, without injection of noise, $\Gamma = 1.20$ while in the presence of noise, that value decreases around $\Gamma = 0.75$ (see Fig. 10). When the coupling parameters are considered non-identical, the stability domain of synchronization states is considerably reduced as the range of instability increases. Moreover, there is no reduction of the critical value of Γ for which all boundaries are almost unchanged. That value remains around 0.5.

5. Conclusions

We have investigated here the modulatory effects of the second range of interaction and local injection on the main dynamical states and their stability boundaries in a network of self-sustained systems. Without and with a locally injected signal in the network, these effects have been analytically investigated for identical and non-identical coupling parameters using the Whittaker method and the Floquet theory. Numerical simulations have been utilized to validate and complement the results of analytical findings. Charts displaying modulatory influences of both the second range of interaction and local

injection on stability boundaries of synchronized states have been drawn. Our investigations revealed that non-nearest neighbors are able not only to influence significantly the stability boundaries of the synchronized states, but also the type of dynamical patterns able to occur in the network. The same finding is true when it comes to local injection. However, the threshold of local injection strength from which stability boundaries remain unchanged can be minimized when the second range of coupling becomes stronger compared to the nearest neighbor coupling. In the case of identical coupling parameters, the threshold's value is considerably reduced when a small amount of Gaussian white noise is also locally injected into the system. But the threshold of local injection strength keeps almost the same value in the case of non-identical coupling parameters without and with a presence of small amount of noise. Thus, injecting a small amount of noise merely disrupts boundaries of stability, but instead, contributes to minimizing energy needed to achieve steady stability boundaries for identical couplings parameters. On the contrary, when it comes to the case of non-identical coupling parameters, adding a small amount of noise into the system leads to a perturbation of stability boundaries. As a matter of fact, domains of synchronization in this case decrease while regions of instability become bigger. Constructing an experimental model of this network to validate these finding would be an interesting task to be performed. Moreover, extending this study to more than four oscillators will be of interest in order to further our understanding of large networks constituted of self-sustained oscillators. As a matter of fact, in the case of a network where only the nearest neighbors coupling is considered and without local injection, it is known that the synchronization domain is inversely proportional to the number of oscillators embedded in the network [18]. On the contrary, the domain of non-synchronization increases with the number of oscillators. Thus, to adding the contribution of non-nearest neighbors in the stability analysis may further reduce regions of full synchronization states while amplifying those of no synchronization. However, expanding the number of oscillators to an arbitrary number N while a signal is locally injected in the network will probably lead to non-trivial and complex modulation of stability boundaries. These boundaries can differ for excitatory coupling (*positive values of coupling strength*) or inhibitory coupling (*negative values of coupling strength*) as reported by a previous study [33]. Addressing this issue will be an interesting task to consider in the future.

Acknowledgement

MAFS acknowledges financial support from the Spanish Ministry of Science and Innovation under Project No. FIS2009-09898.

Appendix A

When N self-sustained oscillators are linked such that, the k th oscillator interacts with $(k - 1)$ th and $(k + 1)$ th, we obtain the following equations.

$$I_k = \frac{1}{L_c} \int (V_k - V_{k+1})d\tau$$

$$I_{k-1} = \frac{1}{L_c} \int (V_{k-1} - V_k)d\tau. \tag{A.1}$$

But when the interaction between the k th, $(k - 2)$ th and $(k + 2)$ th are also considered (with L_{12} the coupling coefficient), we now have:

$$I_{k-2} = \frac{1}{L_{12}} \int (V_{k-2} - V_k)d\tau$$

$$I_k = \frac{1}{L_{12}} \int (V_k - V_{k+2})d\tau, \tag{A.2}$$

and the k th oscillator is described by the following equations:

$$(I_{k-1} - I_k) + (I_{k-2} - I_k) = \dot{i}_L + \dot{i}_C + \dot{i}_k = \frac{1}{L} \int V_k - C \frac{dV_k}{d\tau} - e_1 V_k + e_3 V_k^3. \tag{A.3}$$

The first time derivative of Eq. (A.3) enables us to obtain that the voltage in the capacitor of the k th oscillator is

$$\frac{d^2 V_k}{d\tau^2} - \frac{a_1}{C} \left(1 - 3 \frac{a_3}{a_1} V_k^2 \right) \frac{dV_k}{d\tau} + \frac{1}{LC} V_k = \frac{1}{L_c C} (V_{k-1} - 2V_k + V_{k+1}) + \frac{1}{L_{12} C} (V_{k-2} - 2V_k + V_{k+2}). \tag{A.4}$$

By using the quantities

$$w_e^2 = \frac{1}{LC}, \quad t = w_e \tau, \quad V_k = \sqrt{\frac{e_1}{3e_3}} x_k,$$

the non-dimensional equations of motion are

$$\ddot{x}_k - \mu(1 - x_k^2)\dot{x}_k + x_k = K_1(x_{k-1} - 2x_k + x_{k+1}) + K_2(x_{k-2} - 2x_k + x_{k+2}).$$

$$\mu = e_1 \sqrt{\frac{L}{C}}, \quad K_1 = \frac{L}{L_c}, \quad K_2 = \frac{L}{L_{12}}.$$

References

- [1] Hedley P, Beasley MR, Wiesenfeld K. Phase locking of Josephson-junction series arrays. *Phys Rev B* 1988;38:8712–9.
- [2] Wang SS, Winful HG. Dynamics of phase locked semiconductor laser arrays. *Appl Phys Lett* 1988;52:1774–6.
- [3] Wiesenfeld K, Bracikowski C, James G, Roy R. Observation of antiphase states in a multimode laser. *Phys Rev Lett* 1990;65:1749–52.
- [4] Benford J, Sze H, Woo W, Smith RR, Harteneck B. Phase locking of relativistic magnetrons. *Phys Rev Lett* 1989;62:969–71.
- [5] Glass L, Mackey MC. From clocks to chaos. Princeton: University Press; 1998.
- [6] Levine DS. Neural population modeling and psychology: a review. *Math Biosci* 1983;66:1–86.
- [7] Ermentrout GB, Kopell N. Frequency plateaus in a chain of weakly oscillators. I. *SIAM J Math Anal* 1984;15:215–37.
- [8] Sherman A, Rinzel J, Keizer J. Emergence of organized bursting in clusters of pancreatic β -cells by channel sharing. *Biophys J* 1988;54:411–25.
- [9] Freeman W. Tutorial on neurobiology: from single neurons to brain chaos. *Int J Bifurcation Chaos* 1992;2:451–82.
- [10] Tass P, Haken H. Synchronization in networks of limit cycle oscillators. *Z Phys B* 1996;100:303–20.
- [11] Collins JJ, Stewart IN. Coupled nonlinear oscillators and the symmetries of animal gaits. *J Nonlinear Sci* 1993;3:349–92.
- [12] Strogatz SH. From Kuramoto to Crawford: exploring the onset of synchronization in populations of coupled oscillators. *Physica D* 2000;143:1–20.
- [13] Robertson RM, Pearson KG. Neural circuits in the flight system of the locust. *J Neurophysiol* 1985;53:110–28.
- [14] Collins JJ, Richmond SA. Hard-wired central pattern generators for quadrupedal locomotion. *Biol Cybern* 1994;71:375–85.
- [15] McClellan AD. Organization of spinal locomotor networks: contributions from model systems. *Comments Theor Biol* 1996;4:63–91.
- [16] Woafu P, Enjieu Kadji HG. Synchronized states in a ring of mutually coupled self-sustained electrical oscillators. *Phys Rev E* 2004;69:046206.
- [17] Nana B, Woafu P. Synchronization in a ring of four mutually coupled van der Pol oscillators: theory and experiment. *Phys Rev E* 2006;74:046213.
- [18] Enjieu Kadji HG, Chabi Orou JB, Woafu P. Spatiotemporal dynamics in a ring of N mutually coupled self-sustained systems. *Chaos* 2007;17:033109.
- [19] Yamapi R, Boccaletti S. Active control of the synchronization manifold in a ring of mutually coupled oscillators. *Phys Lett A* 2007;371:48–57.
- [20] Yamapi R, Enjieu Kadji HG, Filatrella G. Stability of the synchronization manifold in nearest neighbor nonidentical van der Pol-like oscillators. *Nonlinear Dyn* 2010;61:275–94.
- [21] van der Pol B. On oscillation hysteresis in a triode generator with two degrees of freedom. *Lond Edinb Dublin Philos Mag J Sci Ser* 1922;43(6):700–19.
- [22] van der Pol B. The nonlinear theory of electric oscillations. *Proc IRE* 1934;22:1051–86.
- [23] van der Pol B, van der Mark J. The heartbeat considered as a relaxation oscillation, and an electrical model of the heart. *Lond Edinb Dublin Philos Mag J Sci Ser* 1928;6(7):763–75.
- [24] Blekhman I. Synchronization in science and technology. New-York: ASME Press; 1988.
- [25] Goldbeter A. A model for circadian oscillations in the *Drosophila* period protein (PER). *Proc R Soc Lond B* 1995;261:319–24.
- [26] Forger DB, Kronauer RE. Reconciling mathematical models of biological clocks by averaging on approximate manifolds. *SIAM J Appl Math* 2002;62:1281–96.
- [27] Hayashi C. Nonlinear oscillations in physical systems. New-York: Mc-Graw Hill; 1964.
- [28] Nayfeh AH, Mook DT. Nonlinear oscillations. New-York: Wiley-Interscience; 1964.
- [29] Losada C, Mazo M, Palazuelos SE, Pizarro D, Marrn M, Velasco JF. Identification and tracking of robots in an intelligent space using static cameras and an XPCP. *Rob Auton Syst* 2013;61(2):75–85.
- [30] Pikovsky A, Rosenblum M, Kurths J. Synchronization: a universal concept in nonlinear sciences. Cambridge University Press; 2002.
- [31] Ma J, Lowe G. Correlated firing in tufted cells of mouse olfactory bulb. *Neuroscience* 2010;169:1715–38.
- [32] Chembo Kouomou Y, Woafu P. Generalized correlated states in a ring of coupled nonlinear oscillators with a local injection. *Phys Rev E* 2002;66:066201.
- [33] Enjieu Kadji HG, Chabi Orou JB, Woafu P. Synchronization dynamics in a ring of four mutually coupled biological systems. *Commun Nonlinear Sci Numer Simul* 2007;13:1361–72.